Bioprinting 17 (2020) e00069

Contents lists available at ScienceDirect

Bioprinting

journal homepage: www.elsevier.com/locate/bprint

Research paper

Multilayered microcasting of agarose–collagen composites for neurovascular modeling

Hossein Heidari, Hayden Taylor *

Department of Mechanical Engineering, 6159 Etcheverry Hall, University of California, Berkeley, CA, 94720, USA

ARTICLE INFO

Keywords:
Hydrogel
Extracellular matrix
In vitro vasculature
Neurovasculature
Agarose
Collagen
Tight junctions
Trans-endothelial electrical resistance

ABSTRACT

The *in vitro* fabrication of vascular networks is one of the most complex challenges currently faced in tissue engineering. We describe a method to create multi-layered, cell-laden hydrogel microstructures with coaxial geometries and heterogeneous elastic moduli. The technique can be used to build *in vitro* vascular structures that are fully embedded in physiologically realistic hydrogels. Our technique eliminates rigid polymeric surfaces from the vicinity of the cells—overcoming a limitation of many microfluidic models—and allows layers of multiple cell types to be defined with tailored ECM composition and stiffness, and in direct contact with each other. We demonstrate channels with internal diameters as small as 175 μm, and agarose–collagen (AC) gels whose Young's moduli range from 1.4–8.3 kPa. We also show co-axial geometries with layer thicknesses as small as 125 μm. One potential application of such structures is to simulate brain microvasculature. Towards this goal, the composition and mechanical properties of the composite AC hydrogels are optimized for cell viability and biological performance in both 2D and 3D culture. Seven-day viability of human microvascular endothelial cells (HMECs) and SY5Y glial cells is found to be maximized with a collagen content of 0.05% (w/v) when agarose content ranges between 0.25% and 1% (w/v). Additionally, we quantify the roles of type I bovine and rat-tail collagen, Matrigel, and poly-D-lysine–collagen–Matrigel coatings in promoting HMEC spreading, proliferation and confluence. 3D triple-layer vascular constructs have been fabricated, composed of a cannular monolayer of HMECs surrounded by two regions of SY5Ys with differing spatial densities. The endothelia are confluent and maintain trans-endothelial electrical resistance (TEER) values around 300 Ω cm^2 over 11.5 days. This prototype opens the way for intricate multi-luminal blood vessels to be fabricated *in vitro*.

1. Introduction

The need for realistic yet scalable methods of culturing three-dimensional vasculature *in vitro* remains one of the greatest current challenges facing tissue engineering. Most applications of tissue engineering (with, *e.g.*, the notable exception of cartilage) call for vasculature in some form [1]. Applications are growing throughout regenerative medicine, drug discovery and screening, and in fundamental disease studies. There has been significant progress in recent years in producing perfusable blood vessels inside microfluidic systems [2]. There remains a need, however, to create functional networks reliably in much larger-volume systems. Certainly, complete synthetic human organs will require the production of complex, branched vessel networks covering volumes of many cubic centimeters and spanning from the arterial (~1 cm) to capillary (≲100 μm) scales. Additionally, an enormous opportunity and challenge lies in the *in vitro* growth of meat for food, which may have the potential to cut greenhouse gas emissions vastly compared to conventional agriculture, to reshape land use, and to address antibiotic resistance [3]. Nascent meat-growing efforts, however, have been hampered by the lack of a vasculature synthesis technique scalable to hundreds of grams of tissue and the centimeter thicknesses needed [4].

1.1. The importance and challenges of fabricating in vitro vasculature

The degree of physiological realism needed in cultured vasculature can be expected to depend on whether the application is scientific, medical, or agricultural. For example, requirements for realistic endothelial permeability are likely to be looser for cultured meat than for drug-screening models. Several common ingredients of successful vasculature growth can, however, be identified. Firstly, the mechanical properties of the extra-cellular matrix (ECM) need to be representative of

* Corresponding author.
E-mail address: hkt@berkeley.edu (H. Taylor).

https://doi.org/10.1016/j.bprint.2019.e00069
Received 26 August 2019; Received in revised form 31 October 2019; Accepted 5 November 2019
2405-8866/© 2019 Elsevier B.V. All rights reserved.

tissue, with the elastic moduli of many soft tissues of interest typically ranging from 1–100 kPa [5]. Secondly, the ECM needs to contain the requisite adhesive protein sequences to promote cell spreading, and needs to allow remodelling as cellular structures emerge. Thirdly, whether vessels are defined 'top-down' in pre-determined geometries, or are allowed to emerge naturally in 3D culture, confluent monolayers of endothelial cells are needed with inter-cellular junctions that offer sufficiently realistic molecular permeability. Hydrodynamic shear stresses on the order of 1 Pa exerted on the internal walls of the endothelia by blood flow are known to drive tight endothelial junction formation [6], and a realistic *in vitro* vasculature model is likely to need to mimic these stresses. The shear stress magnitude can, in fact, vary substantially across different vascular interfaces depending on the flow rates experienced and the physical size of the lumen. With lumen diameters ranging from <10 μm to >10 mm, and with different tissue sites requiring different circulation rates, shear stress values can vary greatly. *In vitro* models usually target physiologic shear stresses ranging from 0.1–1 Pa, corresponding to blood flow rates of 100–200 μL/min which are typical of larger capillaries and small arterioles.

1.2. Particular challenges of modeling the blood–brain barrier (BBB)

Replicating the cerebral vasculature *in vitro* is vital for understanding and conquering brain diseases, but presents particular challenges because of the characteristics of the blood–brain barrier (BBB). Cerebral capillaries have an exceptionally tightly linked layer of endothelial cells surrounded by pericytes and glial cells, yielding far lower molecular permeabilities than found elsewhere in the body. For accurate drug-screening applications in particular, a full model of the cerebral vasculature is desirable, to reproduce active and passive transport across the BBB.

Moreover, brain tissue is among the most compliant of tissues, and its mechanical characteristics are spatially heterogeneous, nonlinear, time-dependent, and directional. They are also challenging to measure, with reported values varying over at least an order of magnitude depending on, *e.g.*, the loading method used and the age of the tissue [7]. For example, Prange and Margulies [8] modelled the instantaneous (pre-relaxation) shear modulus, G, of various *in vitro* samples of dead human and porcine brain tissue to be in the range 130–530 Pa. Taking the tissue to be incompressible for short deformation time-scales, this result corresponds to Young's modulus, E, of 390–1590 Pa ($E = 2G(1+\nu)$ and $\nu = 0.5$). Later work by Gefen and Margulies, however, found that the short-term shear modulus of unconditioned (*i.e.*, previously undeformed), living porcine brain was on average 1875 Pa, corresponding to $E = 5.6$ kPa when incompressibility is assumed [7]. More recently, Budday et al. used nanoindentation to determine bovine white matter to have a Young's modulus of 1.895 ± 0.592 kPa and gray matter a modulus of 1.389 ± 0.289 kPa [9]. Recent measurements of dead human brain tissue also show a strong dependence on location in the brain, with, *e.g.*, shear moduli extracted from simple shear measurements varying from 0.33 ± 0.18 kPa in the *corpus callosum* to 1.06 ± 0.36 kPa in the cortex [10]. Assuming incompressibility, these measurements imply Young's moduli of 0.99 ± 0.54 kPa and 3.18 ± 1.08 kPa respectively. The mechanical properties of brain tissue are a topic of extensive ongoing research, and realistic BBB models need to be able to replicate at least part of the range of cerebral mechanical characteristics.

The challenge of modelling the BBB has inspired a wide range of *in vitro* fabrication techniques [11]. As we discuss next, these can be categorized into (1) "top-down" methods where the geometry of the modelled interface is pre-defined, (2) "bottom-up" methods where materials and cells conducive to 3D vascular growth are placed *in vitro* and conditions are provided for the emergence of vascular structures, and (3) "hybrid" methods that combine deterministic structuring with emergent vascular growth.

1.3. Small-scale, controlled-geometry ('top-down') methods

A common approach to *in vitro* modelling of vasculature has been to produce a simplified interface that captures elements of the specificity of blood vessel walls and can be used for basic transport studies. The early artificial membrane model of Yang et al. [12] immobilized lipids on silica particles to simulate the solubility of candidate drug molecules in cell membranes and hence predict permeability. Yang's model was focused on one particular aspect of cell membrane behaviour and did not incorporate living cells. The 'cone and plate' model of Dewey et al. [6], meanwhile, elucidated the response of vascular endothelial cells to steady shear stresses, without addressing trans-endothelial transport. An early demonstration of a perfusable microvascular network was Ford's co-culturing of brain microvascular endothelial cells with neural progenitor cells on a macroporous polyethylene glycol scaffold [13]: this work provided evidence of the role of neural cells in promoting density of vascularization. However, extensive use has also been made of planar, porous polymeric membranes—widely known as 'Transwell®' inserts—as culture substrates. This convenient fabrication scheme permits co-culture [14–17], and the planar interface aids endothelial transport measurements and imaging.

Nevertheless, to incorporate multiple cell types in precise juxtapositions and to exert continual shear stresses on endothelia, there has been a shift towards on-chip BBB models with integrated microfluidics. Among these models, Griep's 'BBB-on-chip' [18], Booth's 'micro-BBB' [19], and Brown's 'Neurovascular unit' device [20] all sandwiched porous membranes between microfluidic channels to control fluid flow and gain access to both sides of the endothelium. Prabhakarpandian, meanwhile, achieved the same objective with lithographically defined rows of pillars separated by microscopic gaps which effectively served as a vertically oriented porous membrane onto which an endothelium was cultured [21]. This vertical orientation enabled direct imaging of fluorescent molecular diffusion through the cultured membrane. Sudo also used lithographically defined pillars, but to contain a volume of collagen ECM, portions of which were exposed to adjacent microfluidic channels [22]. This exposed material constituted a substantial fraction of the surface area onto which a microvascular endothelium was then cultured. Angiogenesis originating from this endothelium resulted in migration into the 3D matrix. This approach was adapted by Adriani to create a BBB model incorporating neurons, astrocytes and endothelial cells in three adjacent regions [23].

These models have provided the key ingredients for many fundamental studies. In them, however, endothelia are exposed to some materials that are mechanically far stiffer than they would encounter in the body. For example, microfluidic devices, even if injected with ECM, frequently incorporate elastomeric surfaces that are 100–1000 times stiffer than typical ECM; meanwhile, polystyrene is around 10^6 times higher than ECM in elastic modulus. These differences inevitably present a microenvironment—and may lead to cellular behaviour—that is far from physiologically realistic.

1.4. 'Bottom-up' methods harnessing vasculogenesis and angiogenesis

A second approach to *in vitro* modelling of vasculature is to create the conditions for vasculogenesis and angiogenesis, and allow the natural growth of microvascular networks to proceed within a 3D matrix. This approach sacrifices a degree of geometrical control in order to achieve a dense network of vessels with less fabrication complexity. A number of groups have successfully elicited lumen formation within on-chip gel chambers (*e.g.* Ref. [24]). Indeed, this approach has recently been applied to create a BBB model incorporating human induced pluripotent stem cell-derived endothelial cells, human brain pericytes and astrocytes in a fibrin gel [25]. The cellular structures that emerged from this mixture within the gel showed perfusable lumens with pericytes adhering to and surrounding them. Importantly, the seeding of additional endothelia onto the boundaries of the gel region improved perfusability, indicating a role

both for self-assembly and for top-down structuring of cellular constructs.

This type of method offers apparently natural network geometries, but there is still scope for development. Firstly, the emergent networks that have so far been shown are solely *micro*vascular and do not include the larger vessel diameters that would also be needed for the hierarchical, branched vasculature of a complete organ. Secondly, while a reasonable fraction of lumens formed in this way are perfusable, the yield of perfusable structures is far from perfect. The orientation of emergent vessels can be directed to an extent with interstitial flow [24], but researchers are far from being able to create ideal networks in which arteries branch into arterioles and capillaries which then re-merge into venules and veins.

1.5. Hybrid methods combining direct spatial control with emergent cell behavior

The attributes described above suggest a need for a combination of top-down and bottom-up techniques. To this end, an emerging class of bio-printing methods enables spatially controlled placement of ECM material, which can be coupled with self-organization of cells within these deposited regions. These techniques include casting of hydrogel structures around sacrificial [26] or removable [27] lumen-shaped cores, droplet-based dispensing of cell-laden inks [28,29], embedding of spheroids containing multiple cell types into hydrogels surrounded by endothelial cells [30], photolithography- and stereolithography-based patterning of photocrosslinkable hydrogels [31–33], and extrusion printing of hydrogel–cell precursor mixtures [28]. Among these methods, Hinton's 'freeform reversible embedding of suspended hydrogels' ('FRESH') technique combines extrusion printing of structures with a sacrificial scaffold [34], while Song has shown extrusion of a sacrificial channel geometry into a photocrosslinkable ECM [35]. Additive placement of ECM material by any of these methods can provide a more realistic mechanical microenvironment than the injection of gel into microfabricated devices, because the more rigid surfaces of a typical microfluidic device are absent.

These hybrid methods can deliver greater spatial control of the composition of synthetic tissue than purely top-down or bottom-up methods. However, they do have their own limitations. For example, sacrificial molding makes it challenging to define multiple concentric shells and layers—as might be desired in a BBB model—since it is only possible to remove a sacrificial core once. Furthermore, removal of a sacrificial core can be very slow at capillary-scale diameters if the dissolved material must be transported *along* the lumen; on the other hand, transport of dissolved sacrificial material *through* the lumen walls and gel may be a faster option [36].

Inkjet and extrusion-based processes may address the above concerns, and indeed nozzle-based bio-printing and FRESH have been used to produce approximations to a cylindrical vessel with a resolution of a few hundred microns [28,34]. However, when one considers attempting to scale down these processes to print features tens of micrometers in size, the confinement of material and positioning accuracy are expected to become more problematic. The advent of nozzles that can extrude hollow cylindrical tubes of hydrogel will potentially enable lumens to be printed directly [37]. Multi-layered coaxial extrusion methods have begun to emerge, capable of dispensing multiple materials and cell types [38]. However, it is not clear whether branched structures could be formed by coaxial extrusion.

1.6. A multilayer microcasting technique for vasculature

No prior model, then, simultaneously meets the needs for multi-diameter, branched vessels, realistic mechanical properties, realistic cross-sectional geometry, and layering of multiple cell types around the lumen. The fabrication platform that we introduce here, however, does provide a potential route to delivering all of these capabilities. A sequence of casting and thermal gelation steps is used to build multi-layer coaxial structures (Fig. 1a–c). The structures are produced entirely from hydrogels and the sequential casting approach allows multiple coaxial layers to be created with differing hydrogel compositions and cellular contents. In addition to culturing cells in 3D within the hydrogel materials, it is possible to culture 2D cellular monolayers on the surface of the cast hydrogel. Therefore, the technique is ideally suited to modelling the brain microvasculature, in which not only the endothelium but also the surrounding cellular structures are critically important to its function. As a result, this work goes beyond other recent work in which endothelial monolayers were grown inside channels cast in agarose–gelatin composites [39].

We create structures in two halves using convex-geometry molds, and the halves are then bonded together to produce the final enclosed channels (Fig. 1d). In principle, then, the technique can produce arbitrarily arranged networks of channels with spatially varying diameters, provided that the center-lines of all the channels are located within a single plane or can be projected onto a single plane without intersecting each other. Our method's ability to vary channel diameter with position is not easily accomplished with conventional single-layer lithographic techniques, but is important because it enables physiologically realistic flow velocities and hence wall shear stresses to be replicated *in vitro* [40,41] even in complex, branched channel networks.

2. Materials and methods

2.1. Overview of molding process

The technique produces multilayered hydrogel structures by using a sequence of 3D-printed molds (Fig. 1a–c). At each step, the hydrogel material to be cast is first liquefied by heating. In the first step (Fig. 1a), the material is poured into an empty well of a standard polystyrene 12-well plate. The relevant mold is then brought into contact with the liquid to shape it, and the liquid is allowed to cool below its gelation temperature. The mold is then removed. This first step defines the bulk of the device, or the 'background tissue', containing the basic channel geometries. The second and third steps (Fig. 1b–c) define cylindrical shells of hydrogel nested within the channels that have been defined in the first step. In these steps, the liquefied material is dispensed on to the surface of the pre-existing cast structure inside the well. In principle, this procedure could be repeated to create further concentric layers—for example to surround an endothelium sequentially with pericytes, astrocytes and neural tissue in an organized structure. The volume of material dispensed at each step is precisely measured ($\pm$0.05 mL) using a calibrated pipette to achieve the desired layer thickness. The material cast at each step can have a different composition, to tune, *e.g.*, stiffness, cellular adhesive properties, or degradability. The material for any particular layer may also have cells mixed into it while it is liquid.

Layer-to-layer registration at each step is enabled by hydrodynamic forces in the liquefied hydrogel precursor, which act to center a mold's protrusions within previously fabricated hydrogel channels. Additionally, posts incorporated into the molds further enhance registration and enable the two halves of the hydrogel construct to interlock and form fully enclosed, coaxial structures (Fig. 1d). No special surface treatment is needed for the final assembly step: the flat hydrogel surfaces naturally fuse under the action of surface tension. Prior to assembly of the enclosed structures, the two hydrogel castings are removed from their well-plates and transferred to a Petri dish. This step provides lateral access to the fabricated channel for media perfusion and electrode insertion (see Section 2.11). A detailed step-by-step process flow is provided in the Supplementary Information.

2.2. The key role of gelation temperature hysteresis

The process uses agarose–collagen hydrogels, whose gelation characteristics possess a strong temperature hysteresis. This hysteresis enables the preservation of cellular viability during thermal casting, and

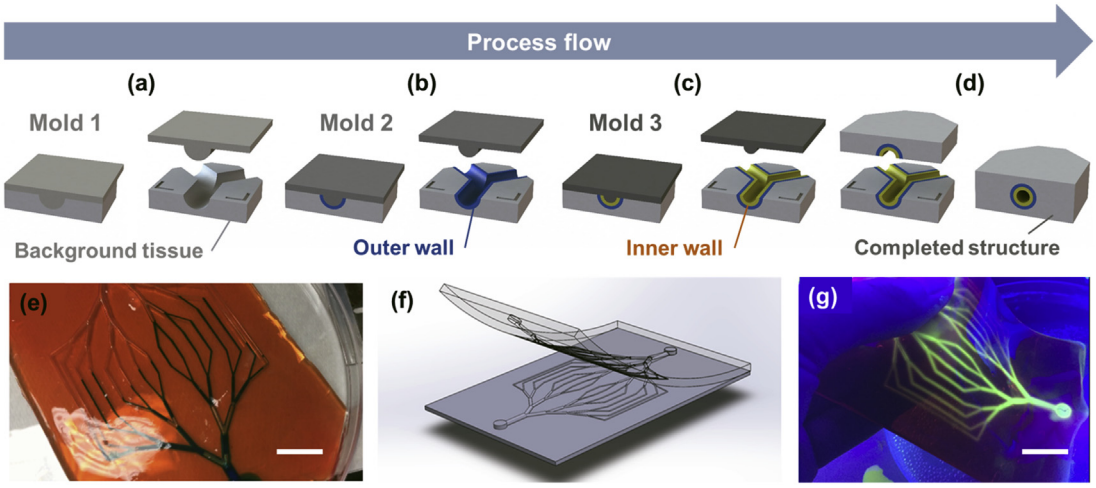

Fig. 1. Fabrication process flow and molding results. Three molding stages (a–c) are shown, each involving pouring, gelation and mold-removal to define a layer from a specific bioink and cell mixture. The first step (a) creates the background tissue; the second (b) defines the outer vessel wall; the third (c) defines the inner wall. The two molded halves of the final structure are then brought together (d) and bond by further gelation. The L-shaped depressions shown in the cast hydrogel layers in (a)–(d) represent layer-to-layer alignment features. (e) A molded, highly branched channel network is perfusable with dyed water. Scale bar: 10 mm. (f) Demolding is carried out via peeling. (g) A molded hydrogel layer is highly compliant. Scale bar: 10 mm.

also allows one hydrogel layer to be cast on top of another without destroying underlying structures. As detailed below (Section 2.4), the gelation temperature of agarose can be tuned in the approximate range 17–40 °C, and the melting temperature of a solid gel is as much as ~40 °C higher than the gelation temperature [42]. In this work, agarose with a gelation temperature of 36 °C is used—*i.e.* just below the physiological temperature of 37 °C at which the devices are to be incubated and used. Prior to casting, the material is melted by immersion in a water bath at 65 °C. It is then allowed to cool to 40 °C before any cells are mixed into it—a temperature that is too high to allow gelation but low enough not to damage the cells. The material is cast, and any underlying, pre-patterned gel structures do not come close to re-melting in this process. The cast layer is then allowed to fall to room temperature to induce gelation. When subsequently raised to the incubation temperature of 37 °C, the structure remains solid.

2.3. Production of molds

For each layer that is to be cast, a 3D computer model of the desired channel geometry is converted into a design for a corresponding, separable two-part mold with the required alignment features. The molds are 3D-printed using an Objet Connex 260 3D inkjet printer with a nominal layer thickness of 16 μm, an in-plane edge-placement precision of approximately ±50 μm, and a minimum in-plane feature size of ~250 μm. The resin used, VeroClear™, is an acrylate-based photocurable material [43]. If finer resolution is needed, alternative mold-making processes such as microstereolithography [44] could be used. In fact, in this work, to probe channel sizes down to diameters of approximately 175 μm, the veins on the underside of a natural tree leaf were used as a mold.

2.4. Agarose–collagen composite hydrogels

Agarose is a thermosensitive natural polysaccharide that consists of copolymers of 1,4-linked 3,6-anhydro-α-L-galactose and 1,3-linked β-galactose [42]. Since the gelation mechanism of agarose is through hydrogen bonding and chain entanglement, the gelation temperature can be configured for the desired application between 17 °C and 40 °C, by tuning the degree of hydroxylethyl substitution. The melting temperature of agarose, meanwhile, is as much as ~40 °C greater than the gelation temperature, displaying useful hysteresis behaviour as explained in Section 2.2 above.

As detailed below, agarose-based hydrogels show exceptional mechanical performance, and can be used to cast sub-millimeter geometries even at very low polymeric concentrations (1% w/v and lower) and elastic moduli (1–10 kPa and less). Pure agarose, however, lacks cell-adhesive domains, resulting in poor cell viability and adhesion in long-term cultures. One way of resolving this biocompatibility issue is by immobilizing adhesion ligands on the crosslinked chains through the activation of hydroxyl groups [45]. An alternative way is the use of binary composites of agarose and other natural biopolymers and ECM proteins [14]. The latter solution offers more degrees of freedom and multi-parameter tunability, via the independent modulation of each component of the hydrogel.

Here, we have studied a wide range of binary agarose–collagen (AC) hydrogels with varying agarose and collagen concentrations (0.25–3.0% w/v and 0–0.2% w/v respectively). We have evaluated them for their mechanical performance, manufacturability and biocompatibility in both 2D (endothelial) and 3D culture. High-melting-point agarose (J.T. Baker, Center Valley, PA, USA) with a gelation temperature of 36 °C was dissolved in sterile Dulbecco's Phosphate Buffered Saline (DPBS, Gibco, Rockville, MD, USA), filter-sterilized, and kept at 40 °C before mixing with type 1 rat-tail collagen (Corning, Corning, NY, USA; supplied at 3–4 mg/mL in 0.02 N acetic acid) that had been diluted in media containing cells as required. The blend was mixed thoroughly and immediately cast as described in Section 2.1.

For each new hydrogel layer that is cast, we can culture cells either as a 2D monolayer on the surface of the solidified hydrogel, or as a 3D cell suspension mixed uniformly into the material prior to casting. Hence, this fabrication process combines 2D and 3D culture modalities into a multi-layered model.

2.5. Cell culture

Human microvascular endothelial cells (HMECs, ATCC CRL-3243, American Type Culture Collection) were cultured in MCDB 131 medium (Thermo-Fisher Scientific, Waltham, MA, USA) supplemented with 10% fetal bovine serum, 10 ng/mL endothelial growth factor (EGF, Thermo-Fisher Scientific), and 1% penicillin/streptomycin at 37 °C in a humidified 5% CO_2 atmosphere. The SH-SY5Y cell line (ATCC CRL-2266, American Type Culture Collection) is a neuroblastoma cell line with epithelial morphology. SY5Y cells were cultured in Dulbecco's Modified Eagle's Medium (Gibco) supplemented with 10% fetal bovine serum (Gibco), 1% non-essential amino acids (NEAA), 1% sodium pyruvate and 1% penicillin/streptomycin (Gibco) at 37 °C in a humidified 5% CO_2

atmosphere. All subcultures were passaged at 80–90% confluence and, throughout the experiments, doubling time was around 48 and 32 h for the SY5Y and HMEC lines respectively. The cells were recovered at this stage after detachment from the culture plates using fresh 0.05% trypsin-EDTA (1X) solution (Gibco) and then either passaged or used in the experiments. In all long-term culture experiments, the medium was refreshed every four days.

2.6. Hydrogel surface coatings

In obtaining an endothelial lumen, the cell adhesion properties of the agarose surfaces play a central role. Unlike many hydrogels, such as collagen, gelatin, and methacrylates of polyethylene glycol, gelatin and hyaluronic acid, whose surface adhesion properties have been studied intensively, agarose hydrogels have not been explored as much. We therefore conducted a study of various surface coatings that would enable cell adhesion and spreading on agarose surfaces. The main surface coatings studied were poly-D-lysine (PDL), Matrigel, collagen, and human-derived fibronectin (hFN). The following protocols were used:

- PDL hydrobromide powder (Sigma-Aldrich, St. Louis, MO, USA) was dissolved in sterile DPBS to a concentration of 0.1 mg/mL and this stock solution was then diluted over a range of concentrations (0.01–0.25 mg/mL) in order to find the optimal coating concentration. The hydrogel substrates were covered with 250 μL/cm^2 of the diluted PDL solutions. The samples were incubated at 37 °C and 5% CO_2 for an hour and then removed from the incubator and washed twice with sterile DPBS, after which they became ready for cell seeding or the application of a secondary coating.
- Matrigel in solution (Corning) was stored at –20 °C, thawed overnight at 2–8 °C and then kept over ice throughout the dilution process. The Matrigel was diluted in sterile DPBS to a range of concentrations (0.1–0.4 mg/mL). The hydrogel substrates were then covered with 50 μL/cm^2 of the diluted solutions, incubated for 30 min, and rinsed with DPBS.
- Collagen type 1 stock solution from one of two sources was diluted at 2–8 °C in sterile tissue-culture-grade deionized water to a concentration in the range 0.5–5.0 mg/mL, and was then applied to the hydrogel surfaces at 200 μL/cm^2. The samples were then incubated for an hour and rinsed with DPBS. The two different collagen sources evaluated were (*a*) rat-tail type 1 collagen (Corning), as used for the AC composites described in Section 2.4, and (*b*) bovine type 1 collagen (PureCol EZGel, Advanced Biomatrix, San Diego, CA), obtained at a concentration of 5.0 mg/mL and a pH of 6.8–7.4.
- The hFN powder (Corning) was dissolved to 1 mg/mL in sterile tissue-culture-grade deionized water, frozen and stored at –20 °C, and then, after re-melting, further diluted to 50 μg/mL and used to coat the surface of the hydrogel substrates at 100 μL/cm^2. The samples were then incubated for 30 min and rinsed with DPBS.
- All coated substrates were then covered with 100 μL/cm^2 of media containing HMEC or SY5Y cells at concentrations of 8.4 × 10^5 and 13.4 × 10^5 cells/mL respectively.

2.7. Mechanical characterization

A Hysitron TI-950 Triboindenter nano-indentation system (Hysitron, Eden Prairie, MN, USA) was used to evaluate the modulus of elasticity of the samples. Hydrogel samples were prepared inside custom-made 3 mm-tall cubic containers and a 1 mm layer of deionized water covered the top surface of the samples in order to keep them hydrated throughout the indentation process. Indentations were made with 50 μm spacing, using a conospherical tip with a radius of 10 μm. The indentation force range was chosen to be 200–600 μN. This force range translated to an average depth of 5000 nm across multiple samples. The Oliver–Pharr method [46] was used to extract the effective elastic modulus, E_{eff}, from the load–displacement data using the following relationship:

$$E_{eff} = \frac{S}{2\beta}\sqrt{\frac{\pi}{A}}$$

where S is the gradient of the initial unloading portion of the load–displacement curve, β is a dimensionless geometry factor taken to equal 1, and A is the tip–sample contact area. Young's modulus, E, of the sample is related to the effective elastic modulus, the indenter Young's modulus E_i, and the sample and indenter Poisson's ratios ν and ν_i respectively by:

$$\frac{1}{E_{eff}} = \frac{1-\nu^2}{E} + \frac{1-\nu_i^2}{E_i}.$$

Since $E_i \gg E$, and the sample is primarily composed of water so that ν during indentation can be assumed to equal 0.5 (signifying incompressibility), Young's modulus of the sample can be taken to equal $0.75E_{eff}$. Young's moduli are reported in the results section.

2.8. Scanning electron microscopy (SEM)

AC hydrogel samples with variations of the two components were prepared in 12-well plates following the same process described in Section 2.4. The samples were then fixed using a 4% paraformaldehyde solution (Electron Microscopy Sciences, Hatfield, PA, USA), and allowed to sit for 20 min. The samples were then cut into 10 mm × 10 mm squares, frozen at –20 °C for an hour and then lyophilized at a vacuum pressure of 0.015 mBar and collector temperature of –52 °C for three days using a benchtop lyophilizer (Labconco, Kansas City, MO, USA). The dried samples were then imaged using a Quanta FEG scanning electron microscope (FEI) at 2–5 keV and 10–22 nA beam current.

2.9. Cell viability assay

A LIVE/DEAD® cell viability kit (Molecular Probes L-3224), whose operation is based on the integrity of the plasma membrane, was used in accordance with the manufacturer's protocol. AC hydrogels with various compositions were synthesized, and cells were kept in culture within these hydrogel environments for a week, while the medium was changed every two days. The viability of cells was evaluated after this seven-day culture period. The dead cells were stained with ethidium homodimer (EthD-1, red stain) and the live cells were stained with calcein AM (CAM, green stain). The samples were then imaged using an Axio Observer D1 fluorescence microscope (Carl Zeiss AG) at excitation/emission wavelengths of 494/517 nm for CAM and 528/617 nm for EthD-1. The images were then analyzed using the NIH ImageJ software to obtain counts of live and dead cells, and viability was calculated as the percentage ratio of live cells to the total number of cells. All viability experiments were repeated for four samples at each ECM composition.

2.10. Cytoskeletal and immunofluorescence staining and imaging

The ZO-1 monoclonal antibody, Alexa Fluor® 594 conjugate (Invitrogen ZO1-1A12) was used for immunofluorescence analysis and visualization of cell junction localization. After removal of the culture medium, the constructs were washed multiple times with DPBS and the cells were fixed with 4% paraformaldehyde for 20 min, then permeabilized with 0.5% Triton™ X-100 (Sigma-Aldrich) for 10 min and blocked with 5% BSA overnight at room temperature. After blocking, the cells were labeled with the ZO-1 antibody, Alexa Fluor® 594 conjugate at 5 μg/mL in 1% BSA and incubated for 3 h at room temperature.

Alexa Fluor® 488 phalloidin (Molecular Probes A12379) was used to visualize the filamentous actin structures of the cells in our 2D and 3D cultures. DAPI (Molecular Probes D1306) was also used to counterstain the nuclei of the cells. Briefly, the culture medium was gently removed from the cellular constructs, and the constructs were carefully washed with DPBS. Cells were fixed using a 4% solution of paraformaldehyde for

20 min after which the solution was removed and the samples were thoroughly washed. The samples were then permeabilized with a diluted solution of 0.5% Triton™ X-100 (Sigma-Aldrich) for 15 min. The phalloidin solution with a 10 μM concentration was then applied and the samples were incubated for an hour in a dark environment. The phalloidin was then removed, the DAPI solution with a 5 μM concentration was added and the samples were incubated for 5 min. The samples were imaged using the Axio Observer D1 fluorescence microscope at excitation/emission wavelengths of 495/518 nm for the phalloidin and 358/461 nm for DAPI.

2.11. Trans-endothelial electrical resistance (TEER) measurement

Trans-endothelial electrical resistance is widely used as a proxy for the tightness of intercellular junctions in an endothelial monolayer [47–49]. TEER measurements were carried out on the vascular constructs as described in Sections 3.5–3.6. The measurement setup consisted of two parallel silver–silver chloride electrodes (A-M Systems 530800). One of the electrodes was carefully guided laterally into the lumen and the other was placed on the outer surface of the construct (Fig. 7a). TEER was measured under DC conditions using an LCR-6000 high precision LCR meter (GW Instek) every three to four days during the 11.5 days after fabrication of the vascular construct.

3. Results and discussion

To identify the most appropriate material compositions for use in multi-layered microcasting, we first determine how elastic modulus depends on gel composition (Section 3.1). We then characterize gel performance by observing three related, but distinct, cell behaviors: *viability* (Section 3.2), *cell-spreading percentage* (Section 3.3), and *proliferation* (Section 3.4). We define viability as the fraction of cells alive after seven days *in vitro*. We define cell-spreading percentage as the fraction of cells exhibiting a clearly non-spherical shape and/or one or more filopodia after two days *in vitro* on the surface of a gel. Proliferation is evaluated qualitatively, in relative terms, and is the extent to which the volumetric density of cells has increased after seven days in 3D culture. The selection of a gel composition for multilayered culture (Section 3.5) needs to consider all three of these characteristics.

3.1. Mechanical characteristics of the hydrogels

We started by investigating the mechanical stiffnesses of agarose hydrogels with no added collagen. As the concentration of agarose was increased from 0.5% to 3.0% w/v, Young's modulus of the gel, measured by nanoindentation, increased nonlinearly from 1.4 kPa to 5.6 kPa (Fig. 2a). The agarose concentration was then fixed at 0.5% w/v and samples were produced with collagen content varying from 0.05% to 0.2% w/v. The addition of the collagen resulted in Young's moduli of the composite hydrogels ranging from 1.4 kPa to 5.1 kPa (Fig. 2b). Meanwhile, fixing agarose content at 1% w/v and varying collagen over the same range yielded Young's moduli ranging from 1.8 kPa to 8.3 kPa.

These results overlap with the large range of measured mechanical properties of brain tissue summarized in Section 1.2 [7–10], indicating that the agarose–collagen system is suitable for BBB modeling. We also note that while the lowest Young's modulus of the gels we made is 1.4 kPa, we have no evidence that this is a lower limit of the material system, and it may well be possible to achieve lower moduli with different compositions.

The results also show that, weight-for-weight, collagen content results in considerably higher moduli than agarose: for example, the addition of 0.2% w/v collagen to a 1% w/v agarose gel increases Young's modulus by 6 kPa, whereas in a purely agarose gel, 3% w/v is needed to approach a modulus of 6 kPa. Elastic modulus alone, however, does not provide a complete picture of mechanical suitability. In preliminary tests, we found that gels composed *only* of collagen—even at polymeric contents as high as 10 mg/mL—readily disintegrated when handled as monolithic layers without any other support. This finding suggests that they would be unable to survive the mechanical manipulation needed to assemble the 3D structures described in Section 3.5. Therefore, the relationship between agarose and collagen appears to be synergistic, with some agarose content being needed for the casting process.

An important difference between the present work and previous techniques is that, in our process, cast gel layers are peeled from the mold and manipulated after casting (Fig. 1e–g) without any additional supporting material present. They thus require greater integrity than gels that are simply injected into microfluidic channels and remain there (*e.g.* Ref. [22]) or gel layers that are cast against and then separated from a mold while being supported by a more rigid material on the back-side (*e.g.* Ref. [50]). In those prior microfluidic devices, plain collagen at ~10 mg/mL was used successfully, but our work has the advantage of being able to produce much larger areas of patterned material that can be directly handled without support. For example, in Fig. 1e–g we show a cast network of branched channels on a 150 mm × 100 mm hydrogel sheet. The ability to handle hydrogel layers without support provides a plausible route to assembling multi-level, deformable tissue and organ models in the future that are beyond the scope of microfluidic gels confined within rigid materials.

To gain better insight into the interactions between agarose and collagen in these hydrogels, we used scanning electron microscopy to image the porous structures of lyophilized samples with various compositions. Agarose structures with very low collagen concentrations (Fig. 2c–e) resemble a tangled mesh of thin, membrane-like material. The mesh density is seen to increase with agarose concentration, resulting in a decrease in the average pore size. The addition of collagen above approximately 0.05% w/v (Fig. 2f), however, results in the appearance of a more 'wireframe'-like network, in which thicker bundles of fibers with diameters as large as a few micrometers have polymeric membranes stretched between them. This organization of the polymeric constituents into thicker wires of material than in the low-collagen cases is expected to reduce buckling and bending of the network, and thus increase the network's specific stiffness considerably.

3.2. Biocompatibility of hydrogels

Cell viability was separately assessed for SY5Y cells (Fig. 3a) and HMECs (Fig. 3b) after seven days in 3D culture in a variety of gel compositions. In the absence of collagen, the hydrogels elicit relatively poor viability—less than 60%—from both cell types. Increasing the collagen content to intermediate concentrations of 0.05–0.1% w/v raises cell viability for both cell lines to 70–85%. Interestingly, however, further increasing the collagen concentration to 0.2% w/v reduces cell viability again, in some cases resulting in lower viability than if collagen were entirely absent.

The existence of an optimal collagen concentration may result from a competition between two effects. On the one hand, it has been shown by Balgude [42] and many others that softer microenvironments—which are provided by lower polymer concentrations—favor cell mobility and proliferation freedom. On the other hand, mechanosensitive pathways such as MAPK influence proliferation, migration, and differentiation, and their activation depends on the there being a high enough density of adhesive protein sequences in the ECM for focal adhesions to form and transmit forces between the nucleus, the cytoskeleton, and the surrounding ECM [51–53]. Collagen provides these adhesive proteins, but increasing its concentration also increases stiffness.

Viability may be further compromised at higher collagen concentrations by the apparent tendency of the material to reorganize itself into larger fibers (noted in Section 3.1 and Fig. 2f). In addition to increasing stiffness, the reorganization into thicker fibers may be expected to result in lower surface-to-volume ratios, which could hide a larger fraction of adhesive proteins from the cells in culture.

Overall, the results show an optimal concentration of 0.5% w/v

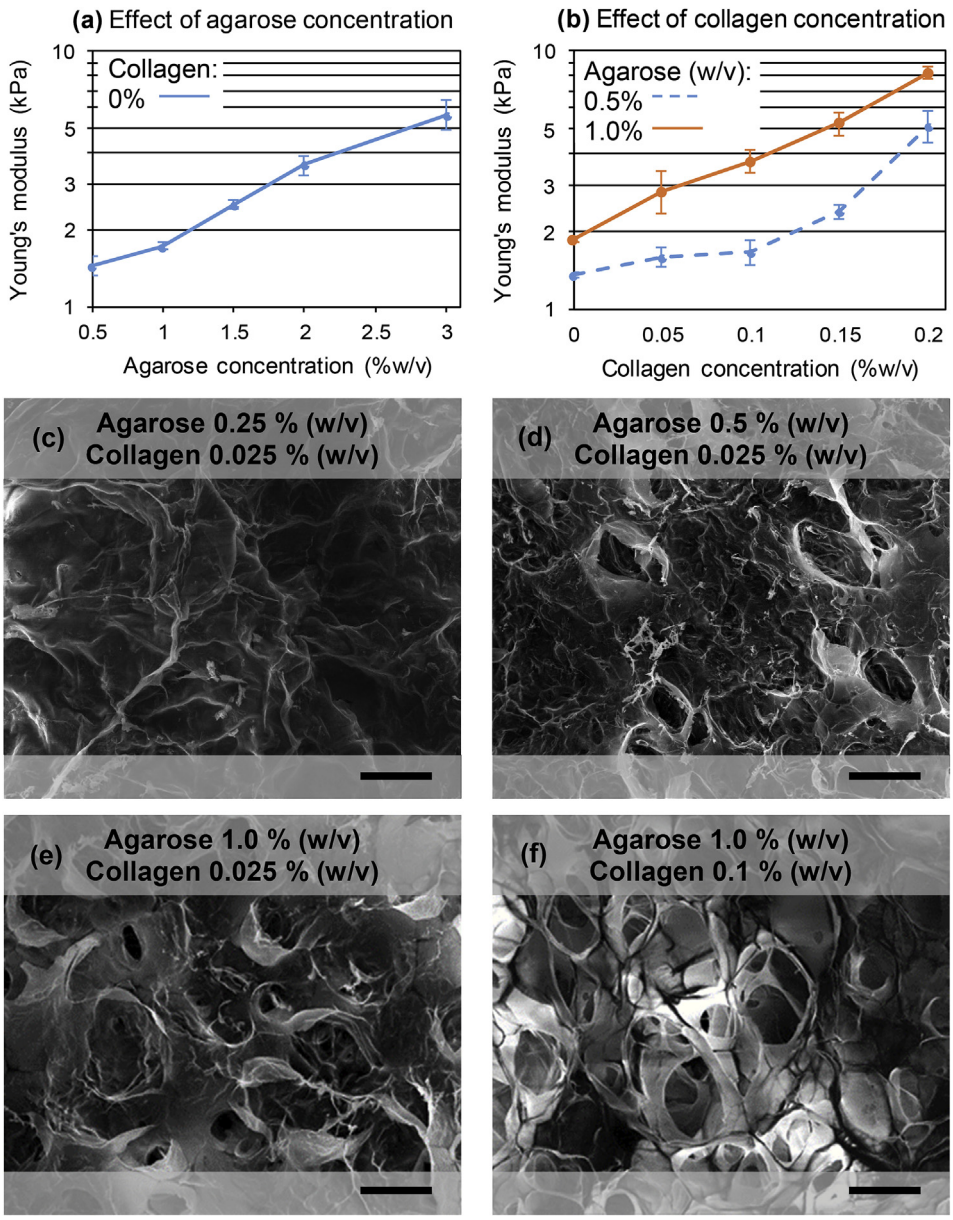

Fig. 2. Mechanical properties and microstructure of agarose–collagen hydrogels. The effects on hydrogel elastic modulus of varying (a) agarose and (b) collagen concentrations show the stronger effect, weight for weight, of collagen concentration. The moduli achieved are comparable to those of *in vivo* cerebral and vascular tissue. Error bars in (a) show ± one sample standard deviation; those in (b) show ± one standard error of the mean, based on the number of measurements shown in the supporting information. Electron micrographs of lyophilized gel structures indicate: (c–e) a reduction in the average diameter of pores at higher agarose concentrations, and (f) added structural support from apparent fiber bundles at higher collagen concentration. Scale bars are all 100 μm.

agarose and 0.05% w/v collagen, at which the seven-day viability values for the SY5Y and HMEC lines were 83% and 85% respectively. These values indicate the suitability of such a gel for 3D culture of both cell lines.

3.3. 2D growth and formation of an endothelium

A successful *in vitro* vascular model requires forming a confluent monolayer of endothelial cells with adequate adhesion to the surface of the ECM on which it is grown. To this end, we have studied the 2D spreading behaviour of HMECs on agarose gels, including with a range of candidate coatings.

We first consider uncoated layers of purely agarose gels with no collagen content and thicknesses between 1 and 4 mm (Fig. 3c). These hydrogel layers were deposited onto relatively rigid polystyrene culture surfaces. Cell spreading after two days *in vitro* is defined as the percentage of cells exhibiting a clearly non-spherical shape and/or one or more filopodia in actin-stained fluorescence micrographs. Higher spreading percentages occur with higher agarose concentrations and thinner layers, both of which can reasonably be supposed to make the hydrogel surface appear stiffer to the HMECs, enhancing migration.

A high spreading percentage does not, on its own, confirm that a confluent monolayer has formed or could form. Neither does it provide direct information about proliferation; it simply shows a propensity of the cells to migrate laterally on a surface, which may ultimately assist monolayer and tight junction formation. In fact, the purely agarose gels did not exhibit confluent monolayer growth after two days, so we investigated (Fig. 3d) the use of coatings following the methods in Section 2.6. For these tests, a 2 mm-thick base gel of 0.5% w/v agarose and 0.05% w/v collagen was used.

With the hFN coating or with a type 1 rat-tail collagen coating applied on its own, HMECs were found not to attach to the surface at all. Meanwhile, a PDL coating dispensed at a concentration of 0.25 mg/mL resulted in just 11% spreading cells after two days (Figs. 3d and 4d). However, when the PDL deposition was followed by either the rat-tail collagen coating or by both rat-tail collagen and 0.2 mg/mL Matrigel coatings in that order (inspired by the work of Han et al. [54]) the spreading fractions increased to approximately 50%. These multi-material coatings in fact resulted in the greatest apparent surface coverage and confluence of HMECs after two days.

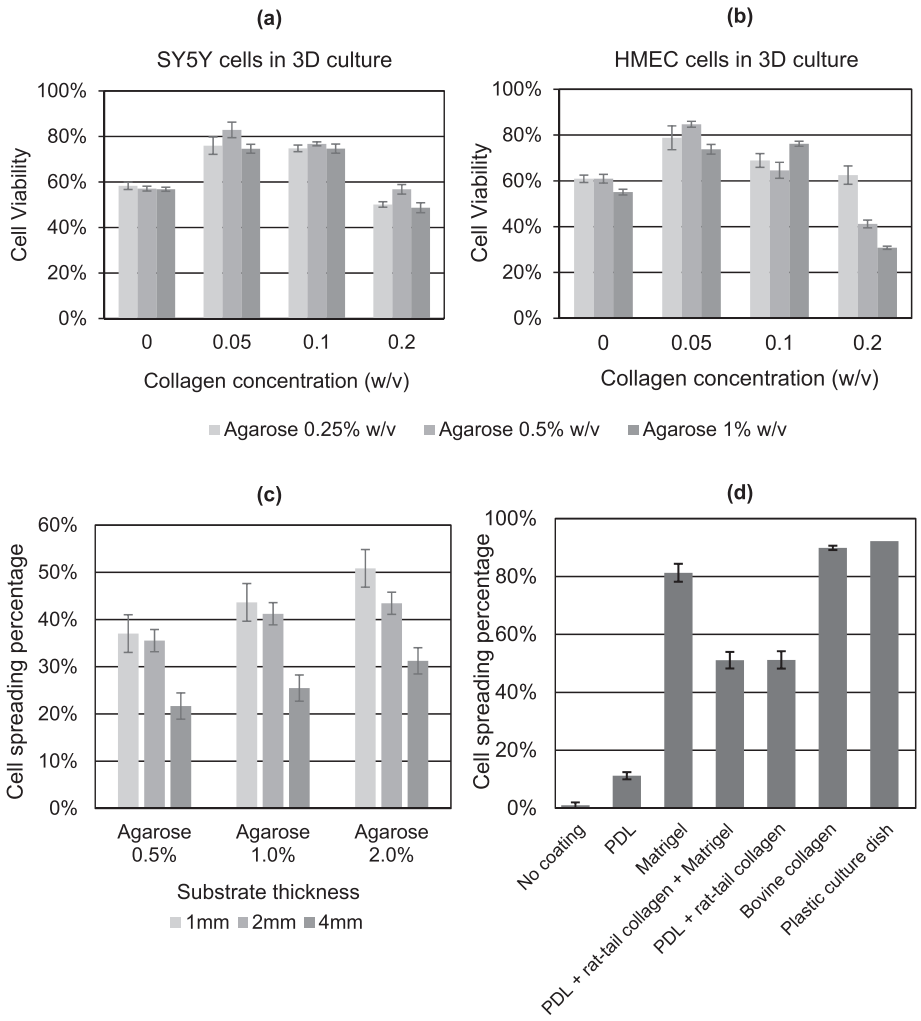

Fig. 3. Cell viability and spreading analysis. Viability values are shown for (a) SY5Y cells and (b) HMECs in 3D culture with varying agarose and collagen concentrations after seven days *in vitro*. Spreading results are evaluated as the percentage of HMECs exhibiting a clearly non-spherical shape and/or one or more filopodia after two days *in vitro*, depending on (c) substrate thickness and agarose content (collagen concentration is zero), and (d) surface coatings on a 2 mm-thick hydrogel layer with 0.5% agarose and 0.05% collagen. Error bars show ±1 standard error of the mean, based on a sample size of four.

The simple application to the base agarose–collagen hydrogel of a Matrigel coating from a 0.2 mg/mL solution (without a preceding PDL deposition) or of a bovine type 1 collagen treatment from a 5 mg/mL solution (Fig. 4e) resulted in even higher two-day spreading percentages: 81% and 90% respectively. They did not, however, correspond to as extensive HMEC surface coverage after two days as was seen with the PDL/rat-tail collagen and PDL/Matrigel/rat-tail collagen coatings. It makes sense that the highest spreading percentages would not necessarily correspond to the greatest confluence at a particular time, because once a layer has become confluent and cells are in lateral contact with each other, they can be expected to cease or reduce their spreading. From these results we find that, of the coatings tried, the multi-material treatments provide the best option to induce rapid confluence of HMEC monolayers.

The above results show that the two different types of collagen coating have elicited rather different HMEC behavior: while the rat-tail collagen coating on its own enabled negligible adhesion, the bovine collagen coating yielded some of the highest spreading percentages. A plausible explanation, other than the differing source of the material, is that the rat-tail collagen was supplied at an acidic pH and was diluted but not fully neutralized before deposition, likely inhibiting significant gelation on the surface. The bovine collagen was supplied at near-neutral pH and may have been able to form a more substantial gel coating during the 1-h incubation period.

We also found that rapid formation of a confluent HMEC monolayer can be promoted by the proximity of SY5Y cells in 3D culture in the hydrogel base layer beneath the developing monolayer (Fig. 4f). This finding is encouraging, because in the neurovascular model described in Section 3.5, an HMEC monolayer grown on the inner surface of the cast lumen is indeed surrounded by glial cells in 3D culture.

While glial cells would typically be grown in 3D, we did also study the 2D growth of SY5Y cells on a 2 mm-thick layer composed of 0.5% w/v agarose and 0.05% w/v collagen, treated with the range of coatings described in Section 2.6. The only coatings that facilitated SY5Y attachment were PDL and PDL/bovine collagen. Favorable adhesion and spreading of SY5Ys were observed for up to two days on a PDL coating that had been deposited from 0.1 mg/mL solution (Fig. 4a–b). After the second day of culture, however, the SY5Ys tended to separate from the purely PDL-coated substrate. This tendency can be attributed to over-confluence of the layer and breakage of the adhesion complexes as a result of layer expansion. The addition of a bovine collagen coating from 5 mg/mL solution on top of the PDL gave better stability to the layer of cells at later stages of culture (Fig. 4c).

3.4. 3D growth and ECM remodelling

Next, we monitored the proliferation, colonization and growth of SY5Y cells in 3D AC hydrogel matrices with varying compositions (Fig. 5). As the agarose concentration is increased from 0.25% w/v to 1.0% w/v, less proliferation is seen after seven days in culture (Fig. 5a–c). Moreover, at the lower agarose concentrations the 3D clusters of cells tend to be larger (Fig. 5d–f), and neurite extensions tend to be longer

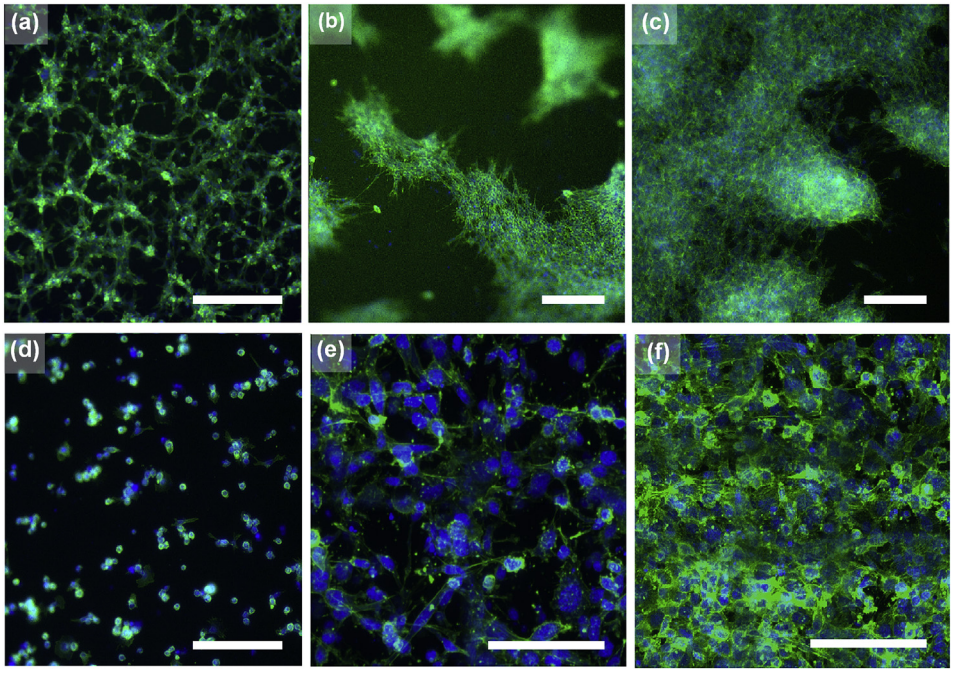

Fig. 4. Effects of modulating the surface adhesion properties of the agarose–collagen hydrogel for SY5Y and HMEC cells. Adhesion of SY5Y cells on the optimal coating (0.1% w/v PDL) on the optimal substrate (2 mm-thick layer of 0.5% agarose and 0.05% collagen): (a) cell adherence after one day *in vitro*; (b) accumulation of cells on the surface after two days *in vitro*; (c) presence of a bovine type 1 collagen coating on top of the PDL enabling stable attachment of the layer of cells even after three days. Adhesion of HMEC cells on different coatings: (d) PDL coating found to be unsuitable for HMEC cells; (e) best cell spreading achieved using a bovine type 1 collagen coating; (f) the same configuration as (e), but with the addition of 3D-cultured SY5Y cells in the gel underneath the endothelium, substantially improving surface coverage and area confluence. All scale bars: 100 μm. All images: green stain: actin; blue stain: nuclei. (For interpretation of the references to colour in this figure legend, the reader is referred to the Web version of this article.)

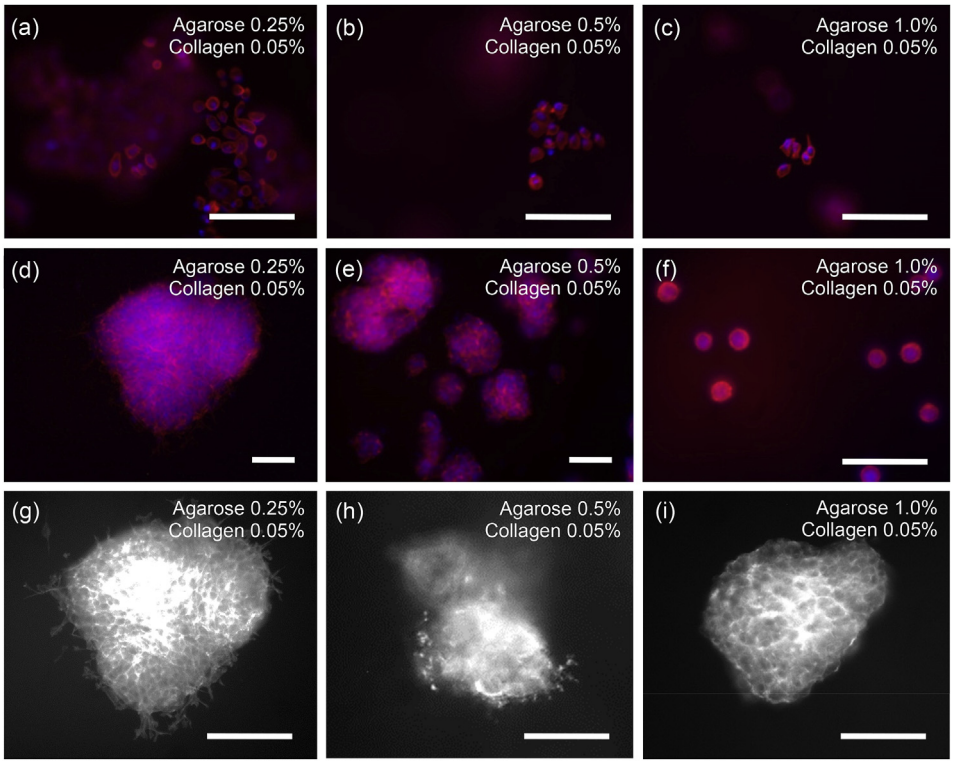

Fig. 5. Expansion and colonization of SY5Y glial cells within 3D agarose–collagen hydrogels: (a–c) overall trend of cell population reduction with the increase in agarose concentration from 0.25% (a) to 1% (c); (d–f) decrease in size of cellular clusters with the increase of agarose concentration from 0.25% (d) to 1% (f); (g–i) decrease in length of neurite extensions with the increase of agarose concentration from 0.25% (g) to 1% (i). Scale bars are all 50 μm. Staining: (a–f): red: actin, blue: nuclei; (g–i): actin. All samples were fixed after seven days in culture. (For interpretation of the references to colour in this figure legend, the reader is referred to the Web version of this article.)

(Fig. 5g–i). Since lower agarose concentrations have been shown to correspond to lower elastic moduli (Fig. 2), these results are consistent with the idea that more compliant microenvironments promote proliferation and mobility [42]. Nevertheless, the strength of the effect of agarose concentration on proliferation, cluster size and neurite growth is striking when it is considered that the seven-day *viabilities* of SY5Y cells remain within the reasonably narrow band of 70–85% for the same range of material compositions: 0.05% w/v collagen and 0.25–1.0% w/v agarose (Fig. 3).

3.5. Fabricated multi-layered 3D vascular constructs

Having demonstrated control of the elastic modulus of AC hydrogels (Section 3.1; Fig. 2), achieved confluent monolayers of HMECs (Section 3.3; Figs. 3 and 4), and produced stable cultures of SY5Y cells (Section 3.4; Figs. 3–5), we were able to synthesize a multi-layered neurovascular model using our new casting technique.

Firstly, we confirmed an ability to produce sub-millimeter enclosed channels in the cast hydrogels. Molds were printed with semi-cylindrical

protrusions having various diameters and a surface roughness of approximately 5 μm peak-to-peak (methods, Section 2.3). With these molds, a single casting step was carried out with 1% w/v agarose solution to produce each half of a hydrogel construct, yielding vessel diameters from 400 to 2000 μm (Fig. 6c–f). To demonstrate even smaller vessel diameters than were featured on our printed molds, we used the vein structure of the underside of a tree leaf as an *ad hoc* mold (Fig. 6a), and were able to form channels with diameters as small as 175 μm (Fig. 6b). FITC fluorescent green dye was mixed into the gel prior to casting all of the samples shown in Fig. 6b–f, to aid visualization.

Next, the multi-layer casting capability was tested (Fig. 6g–i). The first, outermost, casting step (as in Fig. 1a) used a 0.5% w/v agarose, 0.05% w/v collagen composite gel, and was populated with SY5Y cells at a density of 5×10^5 cells/mL. This composition was chosen for the bulk of the device because of its optimal viability performance (Fig. 3a–b) and because it also showed acceptable SY5Y proliferation in 3D culture (Fig. 5). The second casting step (as in Fig. 1b) produced an intermediate layer and was formed from 0.5% w/v agarose, 0.5% w/v collagen without cells. The third and final casting step (as in Fig. 1c) used the same gel composition as the intermediate layer, but with 5×10^6 cells/mL SY5Y cells. This procedure was successfully carried out with molds designed to produce layer thicknesses of 125 μm (Figs. 6g) and 250 μm (Fig. 6h–i). Cross-sections through these structures, with cells fixed after three days *in vitro*, show the successful localization of cells in well-defined layers.

Finally, devices were produced with an integrated endothelial monolayer, bringing together the ingredients of a plausible neurovascular model. These devices involved a simplified casting sequence. The outermost layer of the construct, with an inner diameter of 1 mm, was again made of a 0.5% w/v agarose, 0.05% w/v collagen AC composite gel, and was populated with 5×10^5 cells/mL SY5Y cells. An intermediate layer with an inner diameter of 0.5 mm—and hence a layer thickness of 250 μm—was then cast from a mixture of 0.5% w/v agarose and 0.5% w/v collagen in which had been suspended 5×10^6 SY5Y cells/mL. The higher collagen concentration of 0.5% w/v in this intermediate layer was chosen because, although viability and proliferation would not be expected to be as high as in the optimal 0.05% w/v case, it was expected to provide a somewhat stiffer gel with greater cell-spreading potential during endothelialization, analogous to the results for finite-thickness gels shown in Fig. 3c.

To promote cell spreading further, a bovine type 1 collagen coating was then deposited onto the inside surface of the lumen, following the protocol of Section 2.6. Bovine collagen was applied because, when used with SY5Y cells cultured within the underlying gel, it had been found to support excellent HMEC spreading and confluence (Fig. 4f). HMECs were then seeded inside the lumen from a suspension of 8.4×10^5 cells/mL. After being incubated at 37 °C in a humidified 5% CO_2 atmosphere for 24 h, surplus HMECs were rinsed out from the channel with fresh medium, and incubation continued for a further three days before the structures were fixed and imaged.

A 3D image of the resulting triple-layered lumen was constructed via fluorescence confocal microscopy, and several projections of it are shown in Fig. 6j–k. The majority of the cells in these images are the HMECs lining the lumen. The SY5Y glial cells in the intermediate cast layer can be seen scattered in the region around the lumen. The SY5Y cells in the outermost cast layer have a lower density than those in the intermediate layer and hence appear very sparsely in the images.

To verify that the inner layer is actually a confluent endothelial monolayer with BBB-like integrity, intercellular tight junction proteins ZO-1 were stained and imaged. The top view of a horizontal slice through the lumen of Fig. 6k is shown in Fig. 6l, and it reveals strong ZO-1 expression, indicating the formation of a tightly packed endothelial

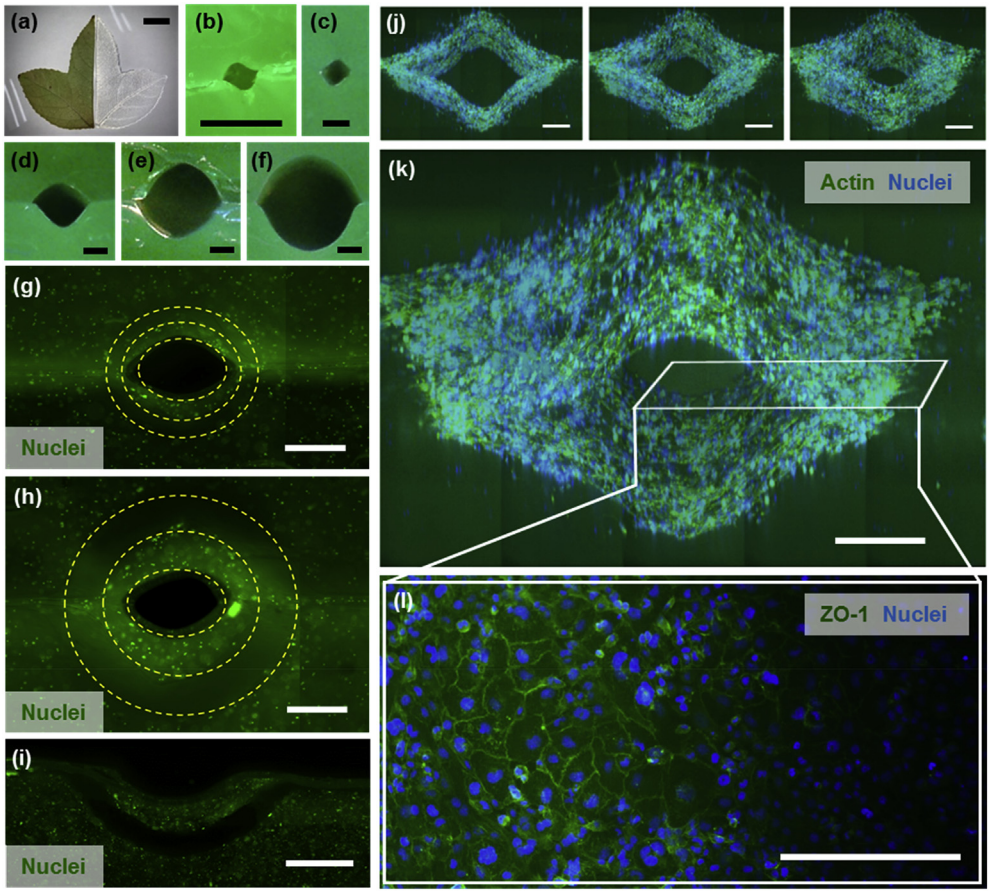

Fig. 6. Fabricated 3D constructs. (a) Visual demonstration of pattern transfer to the gel: in this particular image the vein structure of a tree leaf was used as an *ad hoc* mold. (b–f) Optical micrographs of cross-sections through molded channels with diameters varying from 175–2000 μm: hydrogel is dyed green (the channel in (b) is done using the leaf; all others were done using 3D-printed molds). Fully enclosed channels are formed with 500 μm inner diameter and SY5Y-laden layer thicknesses of (g) 125 μm and (h) 250 μm. (i) Close-up view of a tri-layered construct with 500 μm inner diameter and cell-laden layer thickness of 250 μm, before binding to its opposite half. 3D vascular construct: (j) projections of endothelia with glial cells surrounding the lumen; (k) enlarged view of the same lumen; (l) ZO-1 immunofluorescence micrograph of the endothelial monolayer indicating the tight junction proteins. Scale bars: (a): 10 mm; (b)–(f): 500 μm; (g)–(i): 600 μm; (j)–(l): 100 μm. (For interpretation of the references to colour in this figure legend, the reader is referred to the Web version of this article.)

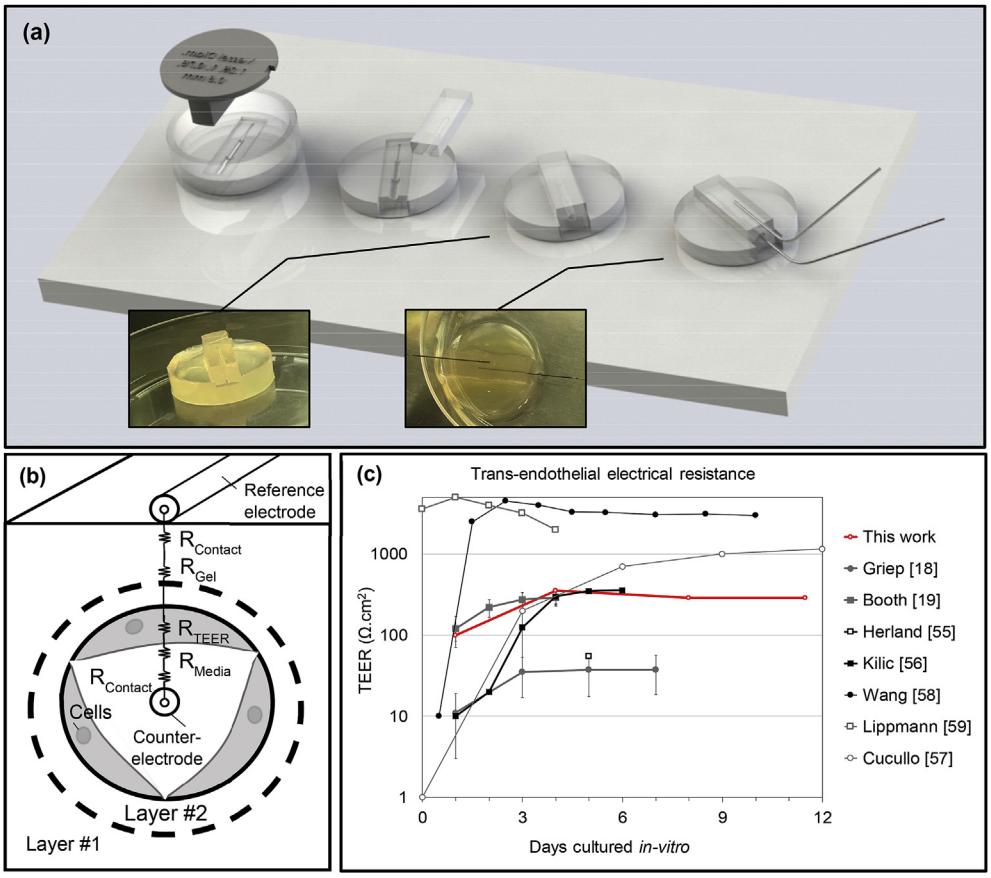

Fig. 7. TEER measurement. (a) Electrode configuration and measurement setup. (b) Schematic of the equivalent circuit adopted for the vascular construct. (c) Progression of TEER values over 12 days for the present work and other reported neurovascular unit models. Error bars for our work (red line) indicate ± one sample standard deviation based on at least four independent measurements from each of two separate devices. Error bars are smaller than the symbols in all but the 1-day case. (For interpretation of the references to colour in this figure legend, the reader is referred to the Web version of this article.)

monolayer after three days *in vitro*.

Fig. 6 shows that the molded geometries are not perfectly circular in cross-section, even though the mold protrusions were designed as half-cylinders. Scanning electron microscopy of a representative 3D-printed mold confirmed that the semi-cylindrical mold protrusions were sharply defined at their bases. It is possible that the shape deviations of the molded hydrogels resulted from imperfect wetting of the mold. If imperfect wetting is responsible, it might be improved by increasing the hydrophilicity of the mold prior to casting, for example via a brief oxygen plasma exposure. Another possible explanation for the shape deviations is that the hydrogel's own surface tension may have led to the rounding of sharp corners after gelation and removal from the mold. This second possible behavior could potentially be pre-compensated for to some extent by modifying the mold geometry to include additional, small recesses along the bases of the semi-circular protrusions, so that when the cast hydrogel retreats under the action of surface tension, its final geometry would more closely approximate the desired shape. Nevertheless, the extent to which any lack of lumen cylindricity affects the permeability and hence usefulness of a BBB model is not clear.

Whether lumens down to 175 μm diameter would be sufficiently small to maintain the viability of fully developed tissue is likely to depend on how densely they could be packed into a fabricated tissue model. It is generally held, based on diffusion considerations, that cells need to be within ~100 μm of a blood vessel to receive adequate nutrients and oxygen, although this requirement certainly varies between different types of tissue. A network of 175 μm-diameter vessels spaced by ~200 μm to meet this notional requirement would contain an exceptionally high volume fraction of lumens, and would therefore likely not be a geometrically realistic representation of natural tissue, but such a network might be appropriate for maintaining the viability of certain *in vitro* models.

Nevertheless, the 175 μm channel dimension demonstrated in this work was simply the smallest size attempted and does not necessarily represent a lower dimensional limit of the process. It is quite conceivable that smaller channels could be fabricated if a suitable mold fabrication technology were to be used, such as photolithography instead of inkjet-based 3D printing. Future work would be needed to establish whether finer features could be preserved throughout the demolding and bonding steps. It may also be possible to induce a small amount of post-fabrication hydrogel swelling (*e.g.* by changing buffer solute concentration) in order to shrink internal channel diameters below those achievable directly by casting.

We also envisage that for more complex tissues the smallest capillaries (down to below 10 μm) would emerge through natural vasculogenesis, in one of two possible ways as other researchers have found (*e.g.* Refs. [24,25]). Smaller vessels could either emerge by sprouting from the larger, deterministically fabricated vessels, or could develop from vascular cells seeded into the 3D extra-cellular matrix surrounding the manufactured lumens. These natural capillary networks would be expected to link to the fabricated lumens, providing an overall network with a defined hierarchy and flow directionality. Such a network would cover the entire spectrum of blood vessel sizes present in actual tissue.

3.6. Trans-endothelial electrical resistance (TEER) measurements

To assess further the integrity of the vascular endothelia described in Section 3.5, TEER measurements were used. TEER is widely used and accepted as a proxy for the impermeability of an endothelium [18,19,55–59]. While it cannot resolve the molecular size-dependence of endothelial permeability in the way that direct observation of fluorescent dye transport can, TEER measurements are relatively rapid and can provide, in a single measurement, information about the entire surface area of an endothelium.

Measurements were made as described as Section 2.11 and illustrated

in Fig. 7a. To interpret these measurements, the device is modelled as five resistive components in series (Fig. 7b). Both the reference and counterelectrodes are made of the same materials and have the same diameter and length, and so are modelled as having equal contact resistances, $R_{contact}$. The multi-layered hydrogel structure of the device is modelled as a single resistance R_{gel}, which reflects the ionic composition of the medium in the pores of the gel, the volume fraction of the gel's polymeric constituents, and its pore geometries. There is no need to distinguish between the various factors contributing to R_{gel} because, as described below, a reference device without the endothelium but with the same gel composition is used to eliminate the contribution of R_{gel}. Meanwhile, R_{TEER} is the transendothelial resistance, which is a significant fraction of the total system's resistance and results from the tight junctional proteins of the endothelium. Finally, R_{Media} represents the resistance of the liquid between the endothelium and the counter-electrode.

In order to isolate the TEER, we first measure the resistance of a hydrogel construct with the intended geometry and composition, but without any cells. We then measure the resistance of the construct including the cells, and compute TEER as the difference between the two measurements. This procedure effectively eliminates the contribution of gel, medium and contact resistances.

To track the evolution and stability of the endothelia over time, TEER measurements were carried out on two distinct chips every three to four days over an 11.5-day period. These measurements exceed the temporal span of TEER measurements taken from most other reported *in vitro* models of the BBB (Fig. 7c). The TEER of our 3D vascular constructs with co-cultured HMECs and SY5Y cells reached a maximum average value of 350 Ω cm^2 after four days. This value reduced to 290 Ω cm^2 after eight days *in vitro* and stabilized at this level until the end of the 12-day culture period. This plateau value significantly exceeds the values obtained in Griep's BBB-on-chip model (33 Ω cm^2) [18] and Herland's 3D BBB model (55 Ω cm^2) [55], and compares well with other pioneering microfluidic neurovascular co-culture models such as Kilic's "Brain-on-chip" (360 Ω cm^2) [56] and Booth's "micro-BBB" (290 Ω cm^2) [19].

The TEER values obtained with our platform indicate utility as a BBB model, although, like many previous BBB models, they lie below physiological values, *e.g.* those of approximately 900–1500 Ω cm^2 reported for rat brain [60]. One possible explanation for the difference is that our results were obtained after culturing in static conditions, whereas the role of hydrodynamically induced shear stress in promoting tight junction formation has been widely demonstrated, *e.g.* in Cucullo's DIV-BBB model [57], where higher and closer-to-physiological TEER values of up to 1200 Ω cm^2 were obtained after 12 days by applying shear stress to the endothelium. Our structures are, fortunately, compatible with continuous perfusion and culturing conditions could be refined accordingly in the future.

Additionally, retinoic acid is known to play an important role in brain vascular development [61] and it has been observed that the addition of retinoic acid to the culture medium can substantially enhance the tightness of the barrier. Considerably higher TEER values have been reported, *e.g.* by Wang (>2000 Ω cm^2) [58] and Lippmann (~5000 Ω cm^2) [59], using retinoic acid. These values may in fact be higher than is physiologically realistic. Significantly, Lippmann's system without retinoic acid resulted in TEER values that fell below 300 Ω cm^2 after less than three days, suggesting that the retinoic acid plays a critical role. Although retinoic acid was not used in the present work, it could easily be incorporated.

4. Conclusions and outlook

The microcasting platform that we have demonstrated here offers a versatile method of fabricating multi-layered cellular structures incorporating two- and three-dimensional culture with a mechanically realistic microenvironment and realistic geometries. Our specific findings are as follows:

- Agarose–collagen hydrogel composites can be produced with Young's modulus in the physiologically relevant range of 1.4–8.3 kPa by varying the agarose content between 0.5 and 3% w/v without collagen, or varying the collagen content between 0 and 0.2% w/v with 0.5% or 1% w/v agarose.
- Viability of both SY5Y and HMEC cells after seven days of culture is maximized in the approximate range 70–80% for a collagen content of 0.05% w/v. Viability does not show consistent trends with respect to agarose concentration in the range examined of 0.25–1% w/v.
- For uncoated composite gels, the fraction of cells exhibiting spreading behaviour (*i.e.* one or more filopodia or an elongated shape) after two days' culture reached a maximum of 40–50% when the thickness of the gel took the smallest value tested, 1 mm, and the agarose content was at the highest value tested, 2% w/v. Both higher agarose concentration and the use of thinner gel layers appear to make the surface seem stiffer to cells, facilitating spreading.
- The percentage of cells spreading after two days can be boosted to above 80% by coating the gel surface with Matrigel. A combination coating of PDL, rat-tail collagen and Matrigel in that order offers a spreading percentage of 50% but superior proliferation and confluence after two days than Matrigel alone.
- The microcasting technique has been demonstrated to produce closed channels with diameters of 175 μm and above. although this dimension was the smallest size attempted and does not necessarily represent a lower limit. Smaller channels are expected to be possible, if a suitable mold fabrication technology such as photolithography is used.
- HMECs cultured onto the surface of an optimized agarose–collagen composite gel (0.5% w/v agarose, 0.5% w/v collagen) under static conditions formed endothelial monolayers that were stable for at least 11.5 days, expressed the tight junction protein ZO-1 strongly, and exhibited TEER of approximately 300 Ω cm^2.

Our results indicate the practicality of using this process for the manufacturing of vasculature. The technique is among the very few fabrication methods that enable the 3D co-culture of multiple cell types in direct contact with each other in controlled juxtapositions. Multilayered microcasting offers two significant advantages over culture within microfluidic devices. Firstly, it is inherently scalable to vascular networks covering areas of many square centimeters. Secondly, the final manufactured structure is composed solely of ECM materials that have sufficient mechanical integrity to survive handling; there is no need for them to be contained by glass, rigid polymers, or elastomers. The formation of a tight endothelial interface after only a few days—and particularly one shown to have a consistent morphology over lateral distances of ~500 μm—demonstrates the immediate usefulness of this fabrication route for rapid generation of microvasculature models under a range of experimental conditions.

In this work we have demonstrated the production of planar networks of channels. We can, however, envisage potential ways to extend the method to form 3D networks of channels. Multiple planar networks of channels could be stacked on top of each other to create thicker 3D tissue. The surfaces of our hydrogels naturally fuse upon contact, which assists us in the encapsulation of lumens and could also assist in the stacking of multiple network levels. Given the geometrical freedom that 3D printing offers for the production of the molds, it may also be possible to incorporate layer-to-layer connection channels in the mold designs. These connection channels could be defined by including vertical posts on the molds, around which the hydrogel precursor solutions would flow during casting to yield hydrogel layers with through-holes. In this way, multilayered micromolding may ultimately offer a systematic route to forming coherent, perfusable 3D channel networks.

Declaration of competing interest

The authors have no competing interests to declare.

Acknowledgements

This work was supported by faculty start-up funding from the U.C. Berkeley Department of Mechanical Engineering. The authors gratefully acknowledge the assistance of the staff of the Biomolecular Nanotechnology Center, the Molecular and Cell Culture Facility, operated by Biosciences Divisional Services, and the Jacobs Institute for Design Innovation, all at U.C. Berkeley. In particular, valuable input from Alison Killilea, Paul Lum, Chris Parsell, Carissa Tasto, and Mary West is acknowledged. H.T. acknowledges helpful discussions with Roger Kamm and the authors acknowledge helpful discussions with Yasaman Daghighi.

Appendix A. Supplementary data

Supplementary data to this article can be found online at https://doi.org/10.1016/j.bprint.2019.e00069.

References

[1] H.-H.G. Song, R.T. Rumma, C.K. Ozaki, E.R. Edelman, C.S. Chen, Vascular tissue engineering: progress, challenges, and clinical promise, Cell Stem Cell 22 (3) (2018) 340–354.
[2] S. Kim, W. Kim, S. Lim, J.S. Jeon, Vasculature-on-A-chip for *in vitro* disease models, Bioengineering 4 (1) (2017) 8.
[3] Don't have a cow, man: the prospects for lab grown meat, Adam Smith Institute, [Online]. Available: https://www.adamsmith.org/research/dont-have-a-cow-man-the-prospects-for-lab-grown-meat. (Accessed 2 October 2018).
[4] K. Kupferschmidt, Lab burger adds sizzle to bid for research funds, Science 341 (6146) (2013) 602–603.
[5] D.E. Discher, P. Janmey, Y. Wang, Tissue cells feel and respond to the stiffness of their substrate, Science 310 (5751) (2005) 1139–1143.
[6] J. Dewey C. F, S.R. Bussolari, J. Gimbrone M. A, P.F. Davies, The dynamic response of vascular endothelial cells to fluid shear stress, J. Biomech. Eng. 103 (3) (1981) 177–185.
[7] A. Gefen, S.S. Margulies, Are *in vivo* and in situ brain tissues mechanically similar? J. Biomech. 37 (9) (2004) 1339–1352.
[8] M.T. Prange, S.S. Margulies, Regional, directional, and age-dependent properties of the brain undergoing large deformation, J. Biomech. Eng. 124 (2) (2002) 244–252.
[9] S. Budday, et al., Mechanical properties of gray and white matter brain tissue by indentation, J. Mech. Behav. Biomed. Mater. 46 (2015) 318–330.
[10] S. Budday, et al., Mechanical characterization of human brain tissue, Acta Biomater. 48 (2017) 319–340.
[11] H. Heidari, H. Taylor, Capturing the physiological complexity of the brain's neurovascular unit *in vitro*, Biomicrofluidics 12 (2018), 051502.
[12] C.Y. Yang, S.J. Cai, H. Liu, C. Pidgeon, "Immobilized Artificial Membranes — screens for drug membrane interactions, Adv. Drug Deliv. Rev. 23 (1) (1997) 229–256.
[13] M.C. Ford, et al., A macroporous hydrogel for the coculture of neural progenitor and endothelial cells to form functional vascular networks *in vivo*, Proc. Natl. Acad. Sci. 103 (8) (2006) 2512–2517.
[14] S. Guo, et al., Neuroprotection via matrix-trophic coupling between cerebral endothelial cells and neurons, Proc. Natl. Acad. Sci. 105 (21) (2008) 7582–7587.
[15] C.M. Garcia, D.C. Darland, L.J. Massingham, P.A. D'Amore, "Endothelial cell–astrocyte interactions and TGFβ are required for induction of blood–neural barrier properties, Dev. Brain Res. 152 (1) (2004) 25–38.
[16] E. Vandenhaute, A. Drolez, E. Sevin, F. Gosselet, C. Mysiorek, M.-P. Dehouck, "Adapting coculture *in vitro* models of the blood–brain barrier for use in cancer research: maintaining an appropriate endothelial monolayer for the assessment of transendothelial migration, Lab. Investig. 96 (5) (2016) 588–598.
[17] A. Appelt-Menzel, et al., Establishment of a human blood-brain barrier Co-culture model mimicking the neurovascular unit using induced pluri- and multipotent stem cells, Stem Cell Reports 8 (4) (2017) 894–906.
[18] L.M. Griep, et al., BBB ON CHIP: microfluidic platform to mechanically and biochemically modulate blood-brain barrier function, Biomed. Microdevices 15 (1) (2013) 145–150.
[19] R. Booth, H. Kim, "Permeability analysis of neuroactive drugs through a dynamic microfluidic *in vitro* blood–brain barrier model, Ann. Biomed. Eng. 42 (12) (2014) 2379–2391.
[20] J.A. Brown, et al., Recreating blood-brain barrier physiology and structure on chip: a novel neurovascular microfluidic bioreactor, Biomicrofluidics 9 (5) (2015), 054124.
[21] B. Prabhakarpandian, et al., SyM-BBB: a microfluidic blood brain barrier model, Lab Chip 13 (6) (2013) 1093–1101.
[22] R. Sudo, et al., Transport-mediated angiogenesis in 3D epithelial coculture, FASEB J. 23 (7) (2009) 2155–2164.
[23] G. Adriani, D. Ma, A. Pavesi, R.D. Kamm, E.L.K. Goh, "A 3D neurovascular microfluidic model consisting of neurons, astrocytes and cerebral endothelial cells as a blood–brain barrier, Lab Chip 17 (3) (2017) 448–459.
[24] Y.-H. Hsu, M.L. Moya, C.C.W. Hughes, S.C. George, A.P. Lee, A microfluidic platform for generating large-scale nearly identical human microphysiological vascularized tissue arrays, Lab Chip 13 (15) (2013) 2990–2998.
[25] M. Campisi, Y. Shin, T. Osaki, C. Hajal, V. Chiono, R.D. Kamm, 3D self-organized microvascular model of the human blood-brain barrier with endothelial cells, pericytes and astrocytes, Biomaterials 180 (2018) 117–129.
[26] L.E. Bertassoni, et al., Hydrogel bioprinted microchannel networks for vascularization of tissue engineering constructs, Lab Chip 14 (13) (2014) 2202–2211.
[27] Y. Shimazu, B. Zhang, Z. Yue, G.G. Wallace, J. Fukuda, Engineering of perfusable double-layered vascular structures using contraction of spheroid-embedded hydrogel and electrochemical cell detachment, J. Biosci. Bioeng. (2018).
[28] S.V. Murphy, A. Atala, 3D bioprinting of tissues and organs, Nat. Biotechnol. 32 (8) (2014) 773–785.
[29] X. Cui, T. Boland, Human microvasculature fabrication using thermal inkjet printing technology, Biomaterials 30 (31) (2009) 6221–6227.
[30] E. Sano, C. Mori, Y. Nashimoto, R. Yokokawa, H. Kotera, Y. Torisawa, Engineering of vascularized 3D cell constructs to model cellular interactions through a vascular network, Biomicrofluidics 12 (4) (2018), 042204.
[31] T.Q. Huang, X. Qu, J. Liu, S. Chen, 3D printing of biomimetic microstructures for cancer cell migration, Biomed. Microdevices 16 (1) (2014) 127–132.
[32] M.S. Hahn, L.J. Taite, J.J. Moon, M.C. Rowland, K.A. Ruffino, J.L. West, Photolithographic patterning of polyethylene glycol hydrogels, Biomaterials 27 (12) (2006) 2519–2524.
[33] Z. Wang, et al., Visible light photoinitiation of cell-adhesive gelatin methacryloyl hydrogels for stereolithography 3D bioprinting, ACS Appl. Mater. Interfaces 10 (32) (2018) 26859–26869.
[34] T.J. Hinton, et al., Three-dimensional printing of complex biological structures by freeform reversible embedding of suspended hydrogels, Science Advances 1 (9) (2015), e1500758.
[35] K.H. Song, C.B. Highley, A. Rouff, J.A. Burdick, Complex 3D-printed microchannels within cell-degradable hydrogels, Adv. Funct. Mater. 28 (31) (2018) 1801331.
[36] Y. Daghighi, H. Heidari, and H. Taylor, "Micro-engineering a platform to reconstruct physiology and functionality of the human brain microvasculature *in vitro*," in Microfluidics, BioMEMS, and Medical Microsystems XVI, 2018, Proc. SPIE, vol. vol 10491, p. 104910N.
[37] W. Jia, et al., Direct 3D bioprinting of perfusable vascular constructs using a blend bioink, Biomaterials 106 (2016) 58–68.
[38] Q. Pi et al., "Digitally tunable microfluidic bioprinting of multilayered cannular tissues," Adv. Mater., vol. 30, no. 43, p. 1706913.
[39] Y. Qiu, et al., Microvasculature-on-a-chip for the long-term study of endothelial barrier dysfunction and microvascular obstruction in disease, Nature Biomedical Engineering 2 (6) (2018) 453.
[40] E. Tzima, et al., A mechanosensory complex that mediates the endothelial cell response to fluid shear stress, Nature 437 (7057) (2005) 426–431.
[41] P.F. Davies, Hemodynamic shear stress and the endothelium in cardiovascular pathophysiology, Nat. Rev. Cardiol. 6 (1) (2009) 16–26.
[42] A.P. Balgude, X. Yu, A. Szymanski, R.V. Bellamkonda, Agarose gel stiffness determines rate of DRG neurite extension in 3D cultures, Biomaterials 22 (10) (2001) 1077–1084.
[43] Vero clear [Online]. Available: http://www.stratasys.com/materials/search/veroclear. (Accessed 26 August 2018).
[44] X. Zheng, et al., Design and optimization of a light-emitting diode projection micro-stereolithography three-dimensional manufacturing system, Rev. Sci. Instrum. 83 (12) (2012) 125001.
[45] Y. Luo, M.S. Shoichet, Light-activated immobilization of biomolecules to agarose hydrogels for controlled cellular response, Biomacromolecules 5 (6) (2004) 2315–2323.
[46] W.C. Oliver, G.M. Pharr, Measurement of hardness and elastic modulus by instrumented indentation: advances in understanding and refinements to methodology, J. Mater. Res. 19 (1) (2004) 3–20.
[47] K. Benson, S. Cramer, H.-J. Galla, Impedance-based cell monitoring: barrier properties and beyond, Fluids Barriers CNS 10 (2013) 5.
[48] B. Srinivasan, A.R. Kolli, M.B. Esch, H.E. Abaci, M.L. Shuler, J.J. Hickman, TEER measurement techniques for *in vitro* barrier model systems, J. Lab. Autom. 20 (2) (2015) 107–126.
[49] Y.B. Arık, et al., Barriers-on-chips: measurement of barrier function of tissues in organs-on-chips, Biomicrofluidics 12 (4) (2018), 042218.
[50] Y. Zheng, et al., *In vitro* microvessels for the study of angiogenesis and thrombosis, Proc. Natl. Acad. Sci. 109 (24) (2012) 9342–9347.
[51] Q. Wu, Y. Zhang, Q. Chen, Indian hedgehog is an essential component of mechanotransduction complex to stimulate chondrocyte proliferation, J. Biol. Chem. 276 (38) (2001) 35290–35296.
[52] D.E. Jaalouk, J. Lammerding, Mechanotransduction gone awry, Nat. Rev. Mol. Cell Biol. 10 (1) (2009) 63–73.
[53] M. Barczyk, S. Carracedo, D. Gullberg, Integrins, Cell Tissue Res. 339 (1) (2010) 269.
[54] S. Han, et al., Constructive remodeling of a synthetic endothelial extracellular matrix, Sci. Rep. 5 (2015) 18290.
[55] A. Herland, A.D. van der Meer, E.A. FitzGerald, T.-E. Park, J.J.F. Sleeboom, D.E. Ingber, Distinct contributions of astrocytes and pericytes to neuroinflammation identified in a 3D human blood-brain barrier on a chip, PLoS One 11 (3) (2016), e0150360.
[56] O. Kilic, et al., Brain-on-a-chip model enables analysis of human neuronal differentiation and chemotaxis, Lab Chip 16 (21) (2016) 4152–4162.

[57] L. Cucullo, et al., Immortalized human brain endothelial cells and flow-based vascular modeling: a marriage of convenience for rational neurovascular studies, J. Cereb. Blood Flow Metab. 28 (2) (2008) 312–328.
[58] Y. I. Wang, H. E. Abaci, and M. L. Shuler, "Microfluidic blood–brain barrier model provides *in vivo*-like barrier properties for drug permeability screening," Biotechnol. Bioeng., vol. 114, no. 1, pp. 184–194.
[59] E.S. Lippmann, A. Al-Ahmad, S.M. Azarin, S.P. Palecek, E.V. Shusta, A retinoic acid-enhanced, multicellular human blood-brain barrier model derived from stem cell sources, Sci. Rep. 4 (2014) 4160.
[60] A.M. Butt, H.C. Jones, N.J. Abbott, Electrical resistance across the blood-brain barrier in anaesthetized rats: a developmental study, J. Physiol. 429 (1) (1990) 47–62.
[61] S. Bonney, et al., Diverse functions of retinoic acid in brain vascular development, J. Neurosci. 36 (29) (2016) 7786–7801.